Journal of Power Sources 183 (2008) 126–132

Contents lists available at ScienceDirect

Journal of Power Sources

journal homepage: www.elsevier.com/locate/jpowsour

Chemical stability and hydrogen permeation performance of Ni–$BaZr_{0.1}Ce_{0.7}Y_{0.2}O_{3-\delta}$ in an H_2S-containing atmosphere

Shumin Fang, Lei Bi, Xiusheng Wu, Haiying Gao, Chusheng Chen, Wei Liu*

Laboratory of Advanced Functional Materials and Devices, Department of Materials Science and Engineering, University of Science and Technology of China, Hefei 230026, PR China

ARTICLE INFO

Article history:
Received 11 March 2008
Received in revised form 30 April 2008
Accepted 1 May 2008
Available online 14 May 2008

Keywords:
Cermet
Ni–$BaZr_{0.1}Ce_{0.7}Y_{0.2}O_{3-\delta}$
Hydrogen separation
Chemical stability
H_2S

ABSTRACT

Composite membranes based on Ni and Zr-doped $BaCeO_3$ are promising for hydrogen separation. Such composites show high proton conductivity and adequate chemical stability in H_2O and CO_2, but may be unstable in H_2S. In this work, the hydrogen permeation performance of Ni–$BaZr_{0.1}Ce_{0.7}Y_{0.2}O_{3-\delta}$ was measured in an H_2S-containing atmosphere at 900 °C. The hydrogen permeation flux began to degrade in 60 ppm H_2S and decreased by about 45% in 300 ppm H_2S. After hydrogen permeation tests, X-ray diffraction analysis revealed the formation of BaS, doped CeO_2, Ni_3S_2 and Ce_2O_2S. Analysis of the microstructure and phase composition, and results of thermodynamic calculations suggest that reaction between H_2S and doped $BaCeO_3$ caused the performance loss of the Ni–$BaZr_{0.1}Ce_{0.7}Y_{0.2}O_{3-\delta}$.

1. Introduction

With the stress of global climate change and the development of fuel cells, hydrogen is expected to be a clean fuel which can substitute for oil-based fuels in the future [1]. The high cost of hydrogen production is a choke point in the process of its commercialization as a fuel. The use of membrane technology for the separation of hydrogen from gases generated by reforming or gasification of fossil fuels and biomass is promising as a low-energy-cost process. As these gas mixtures usually contain H_2O, CO_2 and H_2S, the membranes must be chemically stable in such atmospheres. Dense cermets (ceramic–metal composite) composed of nickel and high-temperature proton conductors such as doped barium cerate ($BaCeO_3$) have been developed as cost-effective materials for hydrogen separation membranes [2]. Ni–$BaZr_{0.1}Ce_{0.7}Y_{0.2}O_{3-\delta}$ (Ni–BZCY) shows rather high performance and adequate stability in H_2O and CO_2 at 900 °C [3,4], but there have been few investigations of its stability and performance in the more acidic H_2S.

Some researchers have studied the chemical stability of $BaCeO_3$ in H_2S. Tomita et al. [5] found that the impedance spectra of $BaCeO_3$ were unaffected in 0–10 ppm H_2S at 800 °C. After studying the chemical stability of $BaCe_{0.85-x}Zr_xY_{0.15}O_{3-\delta}$ (x = 0, 0.3, 0.5 and 0.85) in 5000 ppm H_2S at intermediate temperatures (450–700 °C), Li et al. [6] found that $BaZr_{0.85}Y_{0.15}O_{3-\delta}$ (BZY) was stable in H_2S, whereas $BaCe_{0.85}Y_{0.15}O_{3-\delta}$ (BCY) reacted with H_2S, forming BaS and doped CeO_2. Although BZY has adequate stability, its proton conductivity is about one order of magnitude lower than that of BCY [7], and this is too low for high-drain applications such as fuel cells or hydrogen separation. In addition, H_2S may poison Ni-based cermets by sulfur adsorption on the Ni surface [8–10] or by the formation of nickel sulfides (mainly Ni_3S_2). Sasaki et al. [9] found that 5 ppm H_2S caused a significant decrease in the performance of a fuel cell based on a Ni–YSZ anode at 800 and 1000 °C. Zha et al. [10] showed that the poisoning effect became worse at lower temperatures and attributed the poisoning to sulfur adsorption on the Ni surface, which was favored at lower temperatures. Generally, H_2S may deteriorate the performance of Ni–BZCY by interaction between H_2S, BZCY and Ni. Unfortunately, crude natural gas, coal gas and biogas usually contain high levels of H_2S [6], and thus desulfurization is necessary. For the selection of a cost-effective desulfurization process, it is essential to determine the tolerance of Ni–BZCY to H_2S.

In the work described here, we investigated the hydrogen permeation flux and chemical stability of Ni–BZCY in the presence of H_2S concentrations between 30 and 300 ppm at 900 °C. The mechanism of poisoning was also studied in order to find possible means to improve the tolerance of Ni–BZCY to H_2S.

* Corresponding author. Tel.: +86 551 3606929; fax: +86 551 3601592.
E-mail address: wliu@ustc.edu.cn (W. Liu).

0378-7753/$ – see front matter © 2008 Elsevier B.V. All rights reserved.
doi:10.1016/j.jpowsour.2008.05.015

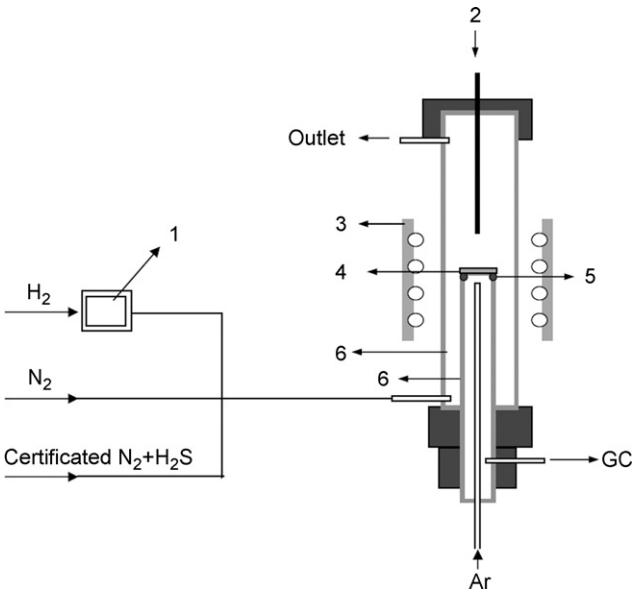

Fig. 1. Experimental arrangement for hydrogen permeation flux measurement: (1) water bath, (2) thermocouple, (3) furnace, (4) sample, (5) glass sealant, (6) alumina tube.

2. Experimental

BZCY powder was prepared via a solid-state reaction method. Appropriate amounts of $BaCO_3$ (AR), ZrO_2 (AR), CeO_2 (AR) and Y_2O_3 (AR) were mixed and ball-milled in alcohol for 24 h. The mixture was then dried and calcined at 950, 1200 and 1400 °C for 10 h with intermittent grinding in an agate mortar. After the presence of a single perovskite phase had been confirmed by use of X-ray diffraction (XRD) patterns, the powder was mixed with Ni powder (>99.5%) in a volume ratio of 70:30. The powder obtained was ball-milled in alcohol for 24 h, dried, ground and then pressed uniaxially to obtain pellets with a diameter of 15 mm. The green pellets were cold isostatically pressed at 300 MPa, and then sintered at 1430 °C for 10 h in 4% H_2 balanced with N_2. The densities of the pellets obtained were measured by the Archimedes method in mercury, and were ~93% of the theoretical density.

The hydrogen permeation flux was measured in a home-built apparatus, shown in Fig. 1. The sintered pellets were polished with 120-, 240- and 600-grit SiC paper in order to make sure that both sides were flat and parallel. The thicknesses of all pellets were about 0.5 mm. Samples were sealed to an alumina tube with a glass ring sealant at 1000 °C for 90 min, after which the temperature was kept at 900 °C. Three samples (labeled 1, 2 and 3) were employed to study the performance and chemical stability for different concentrations of H_2S. Sample 1 was tested in 30 and 60 ppm H_2S, sample 2 was tested in 80 and 100 ppm H_2S, and sample 3 was tested in 120 and 300 ppm H_2S. After the hydrogen permeation flux had stabilized at a low H_2S level, the H_2S was removed. When the hydrogen permeation flux had stabilized again, H_2S was introduced at a higher level.

The feed gas was obtained by mixing 40 ml min^{-1} pure H_2 which bubbled through deionized water at 28 °C, pure N_2 and a certified mixture gas (100 or 503 ppm H_2S in N_2). The total flow rate was 100 ml min^{-1}. The flow rates of pure N_2 and H_2S/N_2 mixture were adjusted by gas gauge to form a feed gas with required H_2S concentration. The nominal compositions of the feed gases with different H_2S levels are shown in Table 1. The sweep gas was high-purity Ar (99.99%) with a flow rate of about 20 ml min^{-1}. The permeated effluent gas was analyzed with a Shimadzu GC-14C gas chromatograph using high-purity Ar as a carrier gas. The hydrogen leakage rate was checked by measuring the leakage of nitrogen, and was below 10% during our measurements. After the tests, the samples were cooled together with the furnace in the testing atmosphere.

Table 1
Nominal composition of feed gases with different H_2S levels

pH_2S (ppm)	pH_2 (atm)	pH_2O (atm)	pN_2 (atm)	Used sample
30	0.4	0.015	0.585	1
60	0.4	0.015	0.585	1
80	0.4	0.015	0.585	2
100	0.4	0.015	0.585	2
120	0.4	0.015	0.585	3
300	0.4	0.015	0.585	3

The phase composition was analyzed by XRD with a Philips X'Pert Pro Super instrument, using Cu Kα1 at 40 kV and 50 mA. The microstructure was observed by SEM with a JEOL JSM-6700F instrument coupled with INCA energy-dispersive X-ray spectroscopy (EDX).

3. Results and discussion

3.1. Time dependence of hydrogen flux in the presence of H_2S

Fig. 2 shows the poisoning processes of samples 1, 2 and 3 in H_2S at 900 °C. The hydrogen permeation flux remained stable when the H_2S concentration was 30 ppm but decreased gradually at higher concentrations (60–300 ppm). After the removal of H_2S, the hydrogen permeation flux always recovered to a value which was slightly higher than the initial flux; thus we have employed the relative hydrogen permeation flux here to avoid overlap. The relative hydrogen permeation flux decreased by about 3, 10, 13, 19 and 45% for 60, 80, 100, 120 and 300 ppm H_2S, respectively. Fig. 3 shows the dependence of the drop in the relative hydrogen flux on the H_2S concentration. It can be seen that the critical H_2S concentration above which the hydrogen flux begins to decrease is ~50 ppm. Thus Ni–BZCY cermet is sustainable in a feed gas containing < 50 ppm H_2S at 900 °C, for example, a mixture produced from natural gas which commonly contains ~1–30 ppm H_2S [11]. Gas mixtures with

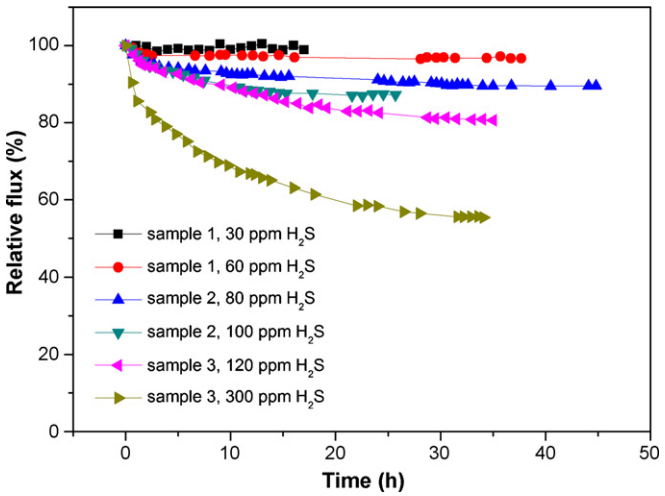

Fig. 2. Time dependence of hydrogen flux in the presence of H_2S, in 0.4 atm H_2 and 0.015 atm H_2O at 900 °C.

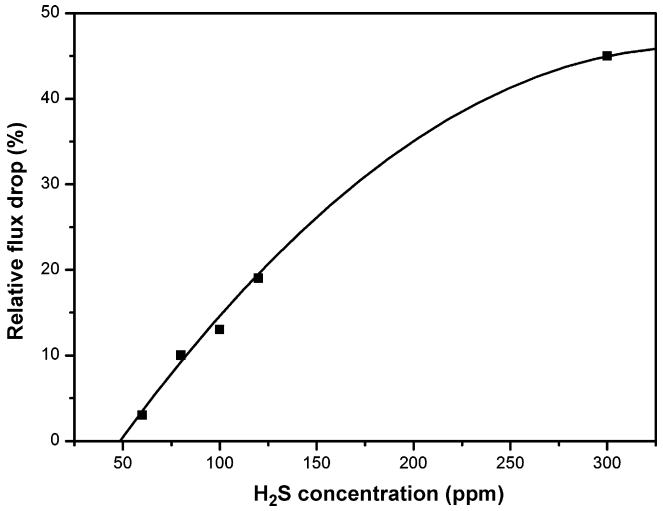

Fig. 3. Dependence of drop in relative hydrogen permeation flux on the H_2S concentration, in 0.4 atm H_2 and 0.015 atm H_2O at 900 °C.

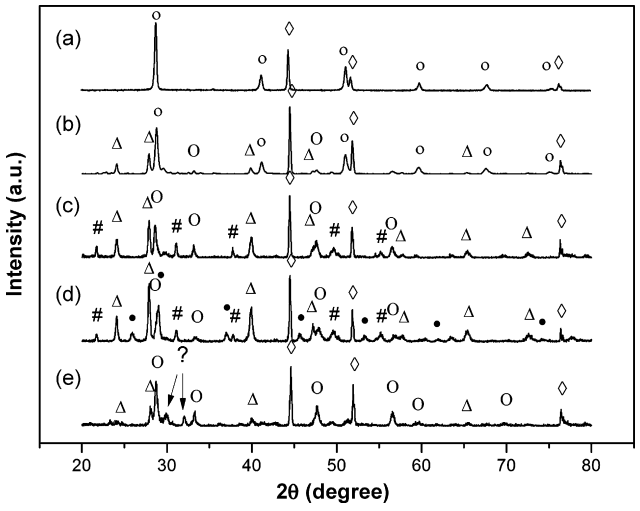

Fig. 5. XRD patterns of Ni–$BaZr_{0.1}Ce_{0.7}Y_{0.2}O_{3-\delta}$ obtained from (a) surface of sintered pellet, (b) feed side surface of sample 1 after exposure to 60 ppm H_2S, (c) feed side surface of sample 2 after exposure to 100 ppm H_2S, (d) feed side surface of sample 3 after exposure to 300 ppm H_2S, and (e) feed side surface of tested sample 3 after reduction in 0.4 atm H_2 and 0.015 atm H_2O at 900 °C for 20 h. (o) BZCY, (◊) Ni, (△) BaS, (○) doped CeO_2, (#) Ni_3S_2, (●) Ce_2O_2S, (?) unknown phase.

higher sulfur levels need to be desulfurized so that an H_2S level of <50 ppm is achieved.

3.2. Regeneration behavior

Fig. 4 shows the regeneration behavior of sample 3. After the introduction of 120 ppm H_2S for 37 h, the hydrogen permeation flux decreased ~19% and then stabilized. When the H_2S was removed for 30 h, the hydrogen permeation fluxes recovered slowly and stabilized at ~102% of the initial value. Similar behavior was observed for sample 2.

3.3. Chemical stability

Fig. 5a shows an XRD pattern of a fresh pellet. The main peaks can be assigned to Ni (JCPDS no. 70-1849) and BZCY, which is similar to $BaCe_{0.9}Y_{0.1}O_{2.95}$ (JCPDS no. 82-2372). Fig. 5b–d shows XRD patterns obtained from the feed side surfaces of samples 1, 2 and 3, respectively, after the tests described above. The peaks for BZCY diminish in Fig. 5b and disappear in Fig. 5c, while the peaks of BaS (JCPDS no. 75-0896), doped CeO_2 (similar to $Y_{0.2}Ce_{0.8}O_{1.9}$, JCPDS no. 75-0175) appear in Fig. 5b and rise in Fig. 5c. The formation of

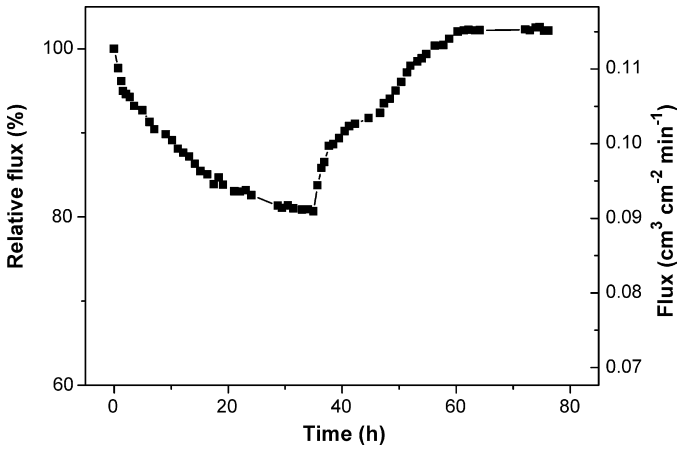

Fig. 4. Sulfur poisoning and regeneration process of Ni–BZCY in 120 ppm H_2S, 0.4 atm H_2 and 0.015 atm H_2O at 900 °C.

BaS and doped CeO_2 is due to reaction between BZCY and H_2S [6]. These results suggest that the reaction is worse at higher H_2S levels. The reaction is incomplete in 60 ppm H_2S but so serious in 100 ppm H_2S that all BZCY on the pellet surface is consumed. Ce_2O_2S (JCPDS no. 26-1085) is found additionally in Fig. 5d, which is attributed to reaction between CeO_2, H_2 and H_2S [6,12,13]. This reaction causes the decrease in the intensities of the peaks corresponding to doped CeO_2 in Fig. 5d. The intensities of the peaks corresponding to BaS continue to increase in Fig. 5d, suggesting that more BZCY reacted with H_2S. As the BZCY on the surface is completely consumed in the sample corresponding to Fig. 5c, this may be related to BZCY below the surface. Ni_3S_2 is found in Fig. 5c and d, which is due to reaction between Ni and H_2S [14]. As a simulation of the regeneration process, one half of sample 3 was reduced in 40% H_2, 1.5% H_2O and residual N_2 at 900 °C for 20 h. An XRD pattern obtained from the feed side surface of the reduced sample 3 is shown in Fig. 5e. The peaks for Ni_3S_2 and Ce_2O_2S vanish and the intensities of the BaS peaks are much weaker than before the reduction. Thus the formation of Ni_3S_2, Ce_2O_2S and BaS is reversible. In addition, the reverse reaction of BaS formation was so slow that part of BaS remained in the sample after treatment in H_2S-free H_2 at 900 °C for 20 h.

Fig. 6 presents SEM micrographs obtained from a polished surface of a fresh sample and from the feed side surfaces of the tested samples 1, 2 and 3. In most of the backscattered micrographs, there are only two phases: a light ceramic phase and a dark Ni phase, which may contain Ni_3S_2 and adsorbed sulfur. However, three phases (light, gray and dark) are observed on the feed side surface of tested sample 1 after exposure to 60 ppm H_2S (Fig. 6b). Fig. 7 shows EDX spectra obtained from the same surface of sample 1. It can be seen that the main component of the light and gray phases is BZCY. It is known that phases with lower average atomic weights are darker in backscattered micrographs. The gray phase contains more sulfur than does the light phase (6% and 2%, respectively, by atomic ratio), and thus it appears darker. Because sulfur exists in the form of BaS on the ceramic surface, the sulfur content indicates the extent of the reaction between BZCY and H_2S. The light phase occupies a larger area than the gray phase, suggesting that only a minor part of the BZCY reacts with H_2S at a level 60 ppm.

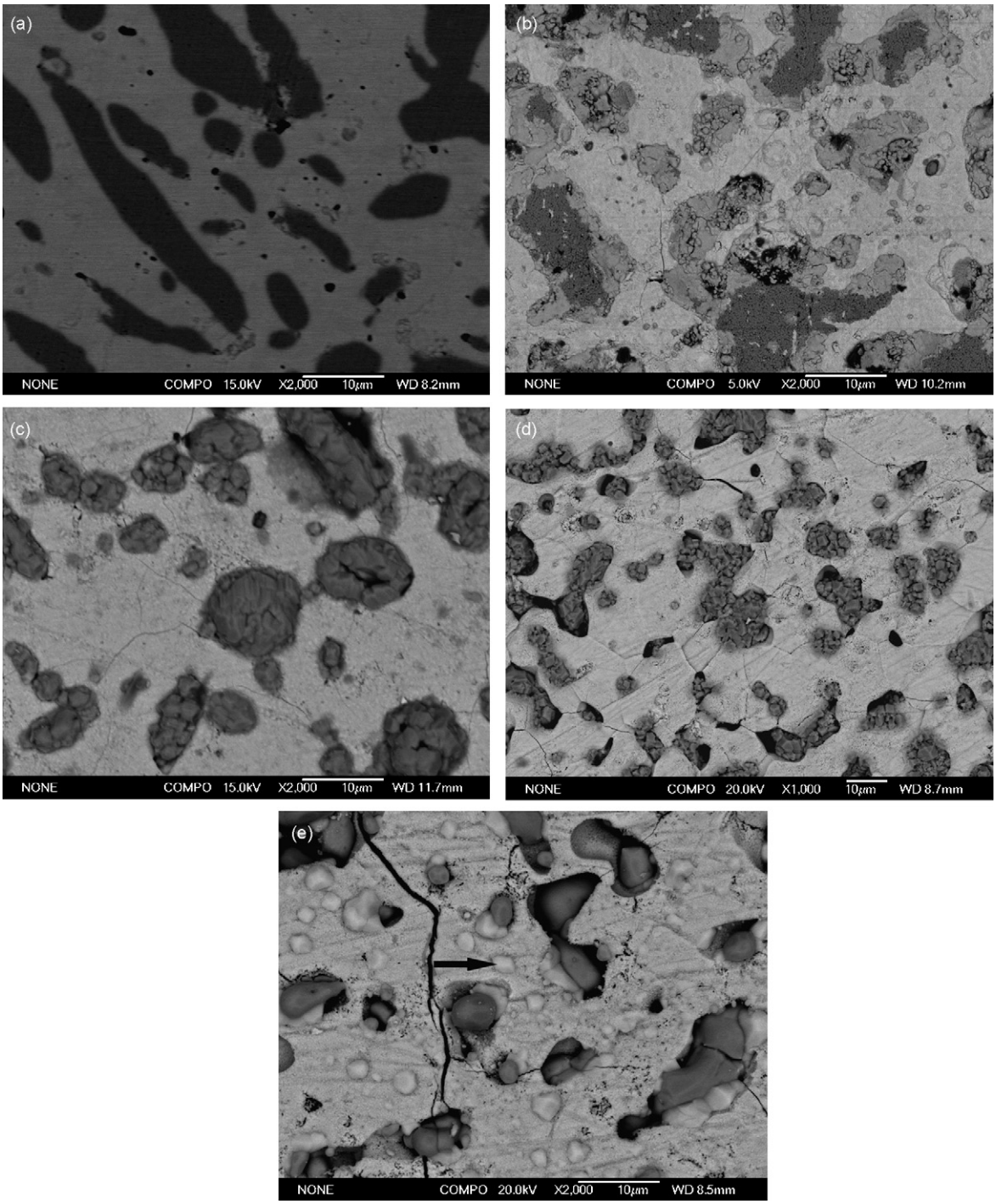

Fig. 6. SEM micrographs (backscattered mode) of Ni–$BaZr_{0.1}Ce_{0.7}Y_{0.2}O_{3-\delta}$ obtained from (a) surface of sintered pellet, (b) feed side surface of sample 1 after exposure to 60 ppm H_2S, (c) feed side surface of sample 2 after exposure to 100 ppm H_2S, (d) feed side surface of sample 3 after exposure to 300 ppm H_2S, and (e) feed side surface of sample 3 after reduction in 0.4 atm H_2 and 0.015 atm H_2O at 900 °C for 20 h.

In Fig. 6c and d, there are no color differences in the ceramic phase, which means that the ceramic phase is uniform after exposure to 100 and 300 ppm H_2S.

The ceramic phase in the fresh sample is dense and crack-free (Fig. 6a). After tests in H_2S-containing atmospheres, cracks are observed on the surfaces of the samples in Fig. 6b–d. When the feed gas contain a higher H_2S level, more cracks appear. When the reactions from $BaCeO_3$ to BaS and CeO_2 and from CeO_2 to Ce_2O_2S are complete, the theoretical volume expansion is 22 and 20%, respectively (calculated on the basis of the information in the JCPDS cards). As the reactions proceed, the volume of the ceramic phase increases, causing severe cracking on the surface. There are many more cracks in Fig. 6d than in c, and thus H_2S can react with more BZCY below the surface, which causes the increase in the intensities of the peaks corresponding to BaS in Fig. 5d. Fig. 6e shows a micrograph of the reduced surface of sample 3. Obviously, the

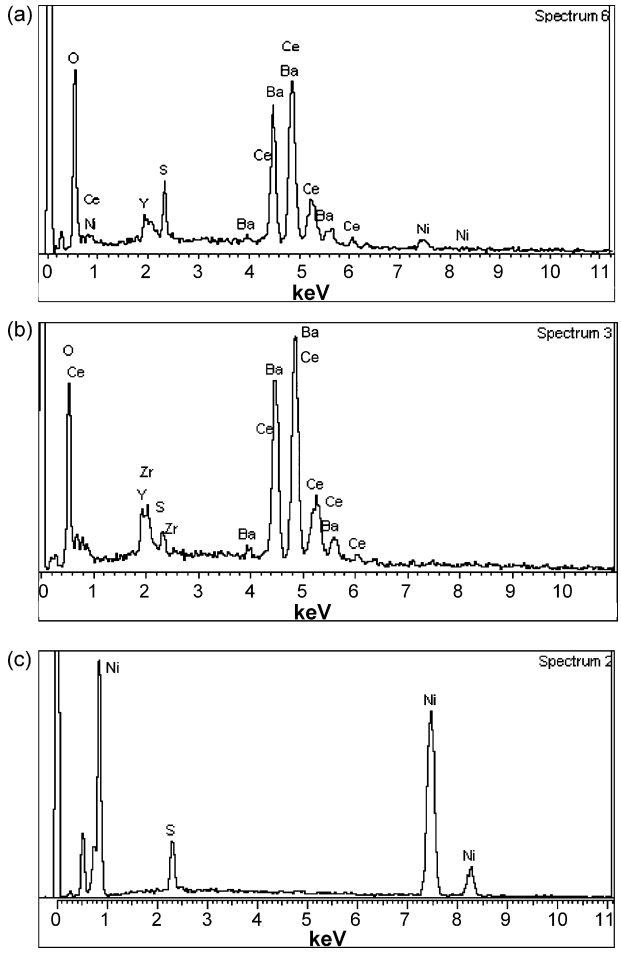

Fig. 7. EDX spectra obtained from the surface of sample 1 after exposure to 60 ppm H_2S. (a) gray phase, (b) light phase, (c) dark phase.

cracks have been preserved after reduction, and some unknown particles (marked by an arrow) have appeared on the surface of the ceramic phase.

The appearance of the planar Ni surface changed greatly after exposure to H_2S. Tiny sphere-like particles appeared on the dark regions of the surface in sample 1 (Fig. 6b). These particles contained Ni and S with an atomic ratio of 88:12 (Fig. 7c), which could indicate Ni together with bulk Ni_3S_2. In the case of samples 2 and 3, the planar Ni surface became granular (Fig. 6c and d). After reduction in H_2 at 900 °C, the rough surface of the dark phase in Fig. 6d became smooth (Fig. 6e); this phase should be Ni, considering the XRD pattern in Fig. 5e.

3.4. Mechanism of sulfur poisoning

Our results show that the hydrogen permeation performance and the microstructure of Ni–BZCY cermets are severely deteriorated by H_2S, but the mechanism of this poisoning is not clear. To our knowledge, H_2S might poison a Ni–BZCY cermet by three routes: sulfide (Ni_3S_2) formation, sulfur adsorption and BaS formation. Peaks corresponding to Ni_3S_2 were observed in the XRD patterns of pellets after testing in 100 and 300 ppm H_2S. If the poisoning is caused by Ni_3S_2 formation, the regeneration process should finish when the Ni_3S_2 has been completely reduced. However, Ni_3S_2 was reduced quickly to Ni (Fig. 5e) whereas the regeneration process takes about 30 h. Thus it is unlikely that Ni_3S_2 formation causes the poisoning. In fact, Sasaki et al. [9] demonstrated that Ni_3S_2 was

Table 2
Thermodynamic properties of the substances involved in reaction (1)

Substance	$\Delta_f H^\circ$ (kJ mol^{-1})	S° (J mol^{-1} K^{-1})	C_p° (J mol^{-1} K^{-1})	Reference
H_2S	−20.6	205.8	34.19	[19]
$BaCeO_3$	−1690.0	144.5	111.91	[20]
H_2O	−241.9	188.8	33.60	[19]
BaS	−460.0	78.2	49.37	[19]
CeO_2	−1089.4	62.3	61.49	[13]

stable only when pH_2S was greater than 1% at 800–1000 °C after studying the Ni–S–O phase diagram. Cheng and Liu [15] reported that Ni_3S_2 formed only in a slow cooling process below 500 °C with pH_2S/pH_2 = 100 ppm. We have also calculated the critical value of pH_2S/pH_2 above which H_2S would react with Ni to form Ni_3S_2, and the result of about 17,000 ppm at 900 °C was much higher than the value obtained in our experiment. Thus the Ni_3S_2 found after testing at 900 °C was formed during the cooling process, and should not affect the hydrogen permeation performance.

Sulfur adsorption may decrease the performance of Ni–YSZ/SDC anodes by decreasing the number of electrochemical reaction sites at relatively low H_2S levels and causing the oxidation of nickel to nickel oxide at higher H_2S levels [9]. The latter is feasible in solid oxide fuel cells (SOFCs) owing to the continuous supply of oxygen ions from the electrolyte, but unfeasible for Ni–BZCY in our reducing atmosphere, and thus the effect of the poisoning caused by sulfur adsorption should be weaker in Ni–BZCY cermets than Ni–YSZ/SDC anodes. In practice, Matsuzaki and Yasuda [16] found that 0.05 ppm H_2S affected the polarization impedance of a Ni–YSZ electrode at 800–1000 °C. A drop in cell performance in several ppm of H_2S at 800 °C has also been reported [9,10,17]. In contrast, the hydrogen permeation performance of Ni–BZCY remained stable in 30 ppm H_2S at 900 °C. The cell voltage of SOFCs based on Ni–YSZ anode has been measured at a constant load of 200 mA cm^{-2} in H_2S-containing atmospheres at 1000 and 800 °C [9,18]. In both cases, the cell voltage decreased with increasing H_2S content in the fuel gas at lower H_2S levels but remained stable above a certain H_2S concentration; this effect was not observed in our experiment. Besides, the recovery in cell performance is usually incomplete in Ni–YSZ-based SOFCs poisoned by sulfur adsorption [10], whereas the hydrogen permeation flux of our Ni–BZCY recovered to ~102% of the initial value. Considering the difference in behavior between Ni–BZCY cermets and Ni–YSZ/SDC anodes, we believe that sulfur poisoning of Ni–BZCY is not dominated by sulfur adsorption on Ni, especially when the H_2S concentration is low.

On the basis of our results from performance measurements and microstructure analysis, we know that the extent of sulfur poisoning increases when the reaction between H_2S and BZCY is reinforced. It is reasonable for us to make an assumption that the reaction between BZCY and H_2S is the main cause of the poisoning at low H_2S levels. In this case, the hydrogen permeation flux will decrease when the reaction starts. Thus it is necessary for us to know the critical conditions for the reaction, which can be obtained by thermodynamic calculations. The reaction between H_2S and doped $BaCeO_3$ is as follows [6]:

$$H_2S(g) + BaCeO_3(s) = H_2O(g) + BaS(s) + CeO_2(s) \quad (1)$$

On the basis of the thermodynamic properties in Table 2, the standard Gibbs free energy change for this reaction is computed to be $\Delta G_T^\circ = -81907 + 23.06T$ J mol^{-1}. The Gibbs free energy change for this reaction is given by the equation:

$$\Delta G_T = \Delta G_T^\circ + RT \ln \frac{pH_2O/p^\circ}{pH_2S/p^\circ}, \quad (2)$$

where p° denotes the standard atmospheric pressure.

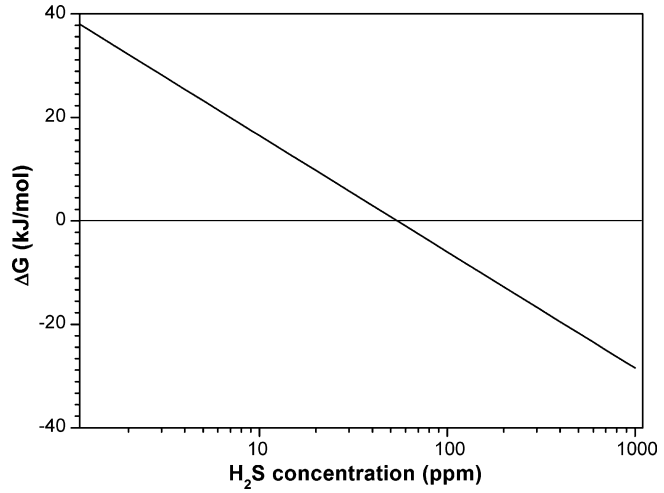

Fig. 8. Dependence of Gibbs free energy change for reaction (1) on H_2S concentrations with 0.015 atm H_2O at 900 °C.

Fig. 8 shows the dependence of the Gibbs free energy change for reaction (1) on the H_2S concentration in an atmosphere containing 1.5% H_2O at 900 °C. Obviously, the critical H_2S concentration for reaction (1) is about 55 ppm, which is very close to the value (~50 ppm) deduced from the experimental data in Fig. 3. The hydrogen permeation performance began to decrease when BZCY started to react with H_2S. The assumption that the poisoning is caused by reaction between H_2S and BZCY is therefore validated by thermodynamic calculations. We suggest a simple mechanism for the poisoning here: when proton-conductive BZCY on the surface transforms into insulating BaS and doped CeO_2, the proton conductivity of the ceramic decreases, which causes a decrease in the hydrogen permeation performance. This mechanism can explain the poisoning behavior very well. When pH_2S was 30 ppm, reaction (1) was thermodynamically unfeasible, and the hydrogen permeation flux remained stable. When pH_2S was 60 ppm, reaction (1) was thermodynamically feasible but very weak owing to the low H_2S content, and only part of the BZCY reacted with H_2S, forming a little BaS and doped CeO_2, causing a slight performance decrease (3%). As the H_2S content increased to 120 ppm, reaction (1) was greatly enhanced and all of the BZCY on the surface was consumed, causing a severe performance decrease (19%). When 300 ppm H_2S was introduced, CeO_2 reacted with H_2S and H_2, forming many cracks. Thus H_2S could react with more BZCY, leading to a more severe performance decrease (45%).

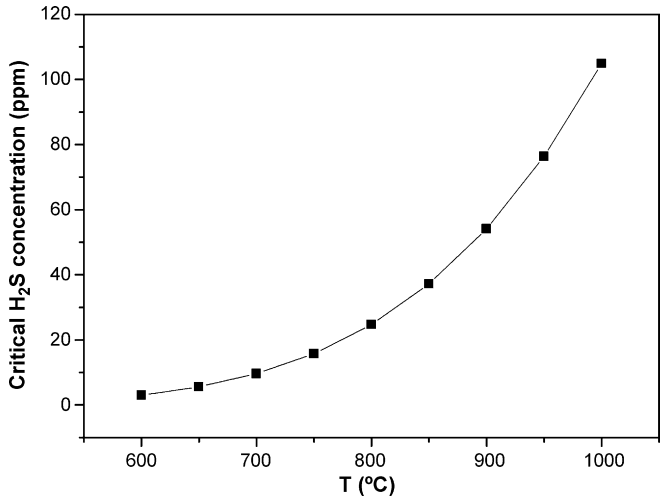

Fig. 9. Temperature dependence of critical H_2S concentration for reaction (1) with 0.015 atm H_2O.

We have also calculated the dependence of the critical H_2S concentration on temperature when pH_2O is 0.015 atm; the result is shown in Fig. 9. The critical H_2S concentration decreases as the temperature falls, indicating the reaction is thermodynamically favored at lower temperatures. The calculated value is 25 ppm at 800 °C. Tomita et al. [5] found that the impedance spectra of $BaCeO_3$ was unaffected in 10 ppm H_2S at 800 °C, which fits well with our calculation results.

It is noticeable that the Gibbs free energy of reaction (1) increases with increasing temperature and pH_2O/pH_2S, and thus the sulfur tolerance of Ni–BZCY is governed by the H_2O partial pressure at any given temperature, such as 900 °C. An increase in H_2O concentration may be effective in weakening the poisoning effect; this can be easily achieved in steam methane reforming.

4. Conclusions

The hydrogen permeation flux of the Ni–BZCY cermet was stable in 30 ppm H_2S, but decreased when the BZCY reacted with H_2S to form BaS and doped CeO_2. The performance loss increased with increasing H_2S concentrations. After removal of H_2S, the hydrogen permeation flux was regenerated completely in a few dozen hours. Microstructure analysis showed that the hydrogen permeation performance decreased significantly when the BZCY reacted seriously with H_2S, and thermodynamic calculations suggest that the hydrogen permeation performance began to decrease when BZCY began to react with H_2S; thus the main cause of the sulfur poisoning of the Ni–BZCY at 900 °C was the reaction between BZCY and H_2S. A cermet membrane of this type can be used sustainably with the products of steam reforming of common natural gas, and its tolerance to H_2S may be improved by increasing the water partial pressure in the feed gas.

Acknowledgements

The authors gratefully acknowledge the support of this research by the Key Program of the Chinese Academy of Sciences under contract No. KJCX1.YW07 and the National High-tech R&D Program of China under contract No. 2007AA05Z157.

References

[1] A.L. Dicks, J. Power Sources 61 (1996) 113–124.
[2] G. Zhang, S. Dorris, U. Balachandran, M. Liu, Solid State Ionics 159 (2003) 121–134.
[3] C.D. Zuo, S.E. Dorris, U. Balachandran, M.L. Liu, Chem. Mater. 18 (2006) 4647–4650.
[4] C.D. Zuo, T.H. Lee, S.E. Dorris, U. Balachandran, M.L. Liu, J. Power Sources 159 (2006) 1291–1295.
[5] A. Tomita, K. Tsunekawa, T. Hibino, S. Teranishi, Y. Tachi, M. Sano, Solid State Ionics 177 (2006) 2951–2956.
[6] J. Li, J.-L. Luo, K.T. Chuang, A.R. Sanger, Electrochim. Acta 53 (2008) 3701–3707.
[7] K. Katahira, Y. Kohchi, T. Shimura, H. Iwahara, Solid State Ionics 138 (2000) 91–98.
[8] N.M. Galea, E.S. Kadantsev, T. Ziegler, J. Phys. Chem. C 111 (2007) 14457–14468.
[9] K. Sasaki, K. Susuki, A. Iyoshi, M. Uchimura, N. Imamura, H. Kusaba, Y. Teraoka, H. Fuchino, K. Tsujimoto, Y. Uchida, N. Jingo, J. Electrochem. Soc. 153 (2006) A2023–A2029.
[10] S.W. Zha, Z. Cheng, M.L. Liu, J. Electrochem. Soc. 154 (2007) B201–B206.
[11] H. Kurokawa, T.Z. Sholklapper, C.P. Jacobson, L.C. De Jonghe, S.J. Visco, Electrochem. Solid-State Lett. 10 (2007) B135–B138.

[12] H.P. He, R.J. Gorte, J.M. Vohs, Electrochem. Solid-State Lett. 8 (2005) A279–A280.
[13] R.M. Fertizz, R.J. Gorte, J.M. Vohs, Appl. Catal. B 43 (2003) 273–280.
[14] J. Dong, Z. Cheng, S.W. Zha, M.L. Liu, J. Power Sources 156 (2006) 461–465.
[15] Z. Cheng, M.L. Liu, Solid State Ionics 178 (2007) 925–935.
[16] Y. Matsuzaki, I. Yasuda, Solid State Ionics 132 (2000) 261–269.
[17] Z. Cheng, S.W. Zha, M.L. Liu, J. Power Sources 172 (2007) 688–693.
[18] A. Norheim, I. Waernhus, M. Brostrom, J.E. Hustad, A. Vik, Energy Fuels 21 (2007) 1098–1101.
[19] J.G. Speight, Lange's Handbook of Chemistry, 16th ed., CD&W Inc., Laramie, Wyoming, 2005, pp. 1.237–1.279.
[20] E.H.P. Cordfunke, A.S. Booij, M.E. Huntelaar, J. Chem. Thermodyn. 30 (1998) 437–447.